RESEARCH ARTICLE

Facile synthesis of highly basic, nanocrystalline Fe₂O₃-NiO composites as promising and durable catalysts for selective dehydrogenation of 2-butanol
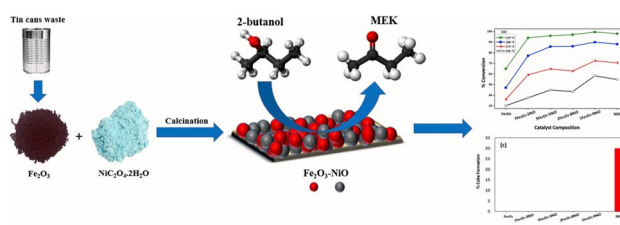
Abouelhassan Ahmed Gomaa[1,2] · Samih Ahmed Halawy[1] · Mohamed Abdelaziz Mohamed[1] · Adel Abdelkader[1]

Abstract

Nanocrystalline Fe_2O_3-NiO composite catalysts were prepared using a sonication-assisted green preparation method. The prepared catalysts were characterized using different techniques, including thermal analyses (TGA/DTA), X-ray diffraction (XRD), Fourier transform infrared (FT-IR) spectroscopy, surface area measurements (S_{BET}), and scanning electron microscopy (SEM). The surface basicity of the prepared catalysts was measured using the temperature-programmed desorption of CO_2 (CO_2-TPD) as a highly acidic probe molecule. The catalytic activity of all the prepared catalysts was tested at a temperature range of 250–325 °C towards the dehydrogenation of 2-butanol to methyl-ethyl ketone (MEK), which is considered a promising fossil fuel alternative and has several industrial applications. The composite catalysts showed better catalytic activity compared to the pure oxides (i.e., Fe_2O_3 and NiO) due to the strong synergetic effect between the two oxides. Fe_2O_3 prevented the coke formation over the surface of NiO by the oxygen-scavenging effect of Fe, which promotes the oxidation of the carbonaceous species and increases the catalyst's resistance to deactivation. The effect of weight hourly space velocity (WHSV) on the catalytic activity was tested over a selected catalyst. In addition, the stability and durability of the catalyst were tested across four successive reaction cycles, demonstrating remarkable performance throughout all the reaction cycles.

Graphical Abstract

✉ Abouelhassan Ahmed Gomaa
abou.elhassan@sci.svu.edu.eg; hussein@dicp.ac.cn

1 Nanocomposite Catalysts Lab., Chemistry Department, Faculty of Science at Qena, South Valley University, Qena 83523, Egypt

2 State Key Laboratory of Catalysis, Dalian Institute of Chemical Physics, Chinese Academy of Sciences, Dalian 116023, China

Introduction

The growing demand for green and sustainable energy sources has significantly increased the interest in the catalytic conversion of biomass, as renewable feedstocks, into fossil fuel alternatives (Kumar and Gayen 2011; Gao et al. 2019; Li et al. 2020b; Li et al. 2001). One of the biggest scientific challenges nowadays is the development of innovative and durable catalytic systems capable of achieving high conversion rates of biomass resources into value-added products. 2-butanol has been recognized as a significant

new-generation biomass platform molecule, demonstrating unique advantages including high calorific value, affordable sources of raw materials, and environmental friendliness compared to traditional bio-methanol or bio-ethanol (Kumar and Gayen 2011; Bharathiraja et al. 2017; Gao et al. 2019; Li et al. 2020a; Li et al. 2001). The selective dehydrogenation of 2-butanol to methyl ethyl ketone (MEK) is considered an important industrial target due to the wide range of industrial applications of MEK (Fang et al. 2009; Varma et al. 2024). MEK serves as a solvent in paints, dyes, and adhesives, especially for polyvinyl chloride pipes and magnetic tapes. In addition, MEK is utilized in the pharmaceutical refining industries and used as a solvent for fats, waxes, oils, and resins. Furthermore, MEK can be used as a precursor for the production of methyl ethyl ketone peroxide (Zhenhua et al. 2006; Bolder et al. 2008; Zhang et al. 2024). Recently, MEK has been introduced as a promising biofuel for spark ignition engines with unique characteristics. Compared to ethanol, MEK has the same engine efficiency, higher heat of combustion, better cold-start characteristics, less oil dilution, and lower emissions of hydrocarbons. These characteristics of MEK contribute to decreasing the global warming and climate change effects on our planet (Hoppe et al. 2016). According to these reasons, MEK is considered an attractive candidate in the supply of chemicals or biofuel, where the global marketing for MEK was valued in 2015 at approximately 2.6 billion USD and is anticipated to reach 4.0 billion USD by 2025 (Halawy et al. 2021). MEK can be produced through the dehydrogenation of 2-butanol over basic solid catalysts (Geravand et al. 2015). There are two ways for dehydrogenation of 2-butanol: liquid dehydrogenation and gas phase dehydrogenation. Gas phase dehydrogenation is widely employed on an industrial scale due to the relatively low investment requirements and the straightforward process flow. The enhancement of catalyst activity, selectivity, and durability is the primary key to driving industrial technological development. In the case of the production of MEK through gas phase dehydrogenation, the main challenge researchers faced was the rapid deactivation of the catalyst due to coke formation on the catalyst surface, where carbon deposition not only degrades catalyst performance but also results in severe pressure drops due to reactor clogging (Guan et al. 2024). The coke formation phenomena at the catalyst surface resulted mainly from the deposition of carbonaceous species, especially at elevated reaction temperatures (Zhenhua et al. 2006). Geravand and his co-workers prepared nanosized Cu/SiO$_2$ catalysts using various precursors and different preparation methods to produce MEK by 2-butanol dehydrogenation. They observed that the catalysts experienced deactivation, which they attributed to the coke formation phenomena, which was detected using FT-IR spectroscopy (Geravand et al. 2015). Gaigneaux and his co-workers studied the dehydration-dehydrogenation of 2-butanol over

a mechanical mixture of Sb$_2$O$_4$ oxide with SnO$_2$ or MoO$_3$ oxides at low temperatures. They found that both mixtures exhibited better catalytic performances than the pure oxides. They attributed the synergetic effects between the phases to the occurrence of a remote-control mechanism acting via the migration of spillover oxygen species. According to Gaigneaux and his co-workers, the spillover creates new acid sites on MoO$_3$, regenerates the reduced deactivated redox sites on both SnO$_2$ and MoO$_3$, and inhibits the coke formation during the reaction (Gaigneaux et al. 1997). Pischetola et al. (2020) prepared a series of Au/CeO$_2$ + Cu/Oxide mixtures, which promoted the exclusive formation of MEK, and found that the catalyst surface was completely covered by coke deposits. In addition, it was reported that using different morphological structures of NiO catalysts, including hierarchical and nanorods, for 2-butanol dehydrogenation to MEK was accompanied by rapid catalyst deactivation, especially at high reaction temperatures, due to coke formation (Halawy et al. 2018; Gomaa et al. 2021). Kayo and his co-workers, as well as Gomaa and his co-workers, studied the effect of different preparation methods of iron oxide on its catalytic activity towards MEK production through the dehydrogenation of 2-butanol. Although the catalytic activity of these iron oxides towards 2-butanol dehydrogenation was lower compared to NiO, they demonstrated better stability as no coke formation was observed on the catalyst surface (Kayo et al. 1983; Gomaa et al. 2023).

In two previous separate studies, we investigated the catalytic activity of both NiO and Fe$_2$O$_3$ toward the dehydrogenation of 2-butanol (Gomaa et al. 2021, 2023). It was found that, although pure NiO has high catalytic activity and high selectivity to MEK, it suffered from rapid catalytic deactivation due to the coke formation on its surface, which reached 30% of its original weight. In contrast, no coke formation was observed in the case of Fe$_2$O$_3$, which shows lower catalytic activity compared to NiO. In the present study, we aim to fabricate a composite consisting of both NiO and Fe$_2$O$_3$ oxides for the dehydrogenation of 2-butanol to combine the advantages of the two oxides. The study will focus on the effect of the mixing ratio on the catalytic activity of NiO-Fe$_2$O$_3$ composite towards the dehydrogenation of 2-butanol. Additionally, a selected catalyst will be chosen for the study of some kinetic parameters.

Experimental

Materials

Tin can waste, and chemicals include nitric acid (HNO$_3$, Merck, 55%), ammonium hydroxide (NH$_4$OH, Merck, 35%), nickel oxalate dihydrate (denoted as Ni-Oxal), and 2-butanol (Fluka).

Preparation of pure NiO and Fe_2O_3

To prepare NiO nanorods, as mentioned in our previous study, nickel oxalate dihydrate $NiC_2O_4.2H_2O$ powder was mixed with a small amount of deionized water and placed in an ultrasonic bath at 70 °C until dryness. The resulting material was dried at 120 °C for 24 h and subsequently calcined in static air for 2 h at 400 °C (Gomaa et al. 2021). To prepare iron oxide, as mentioned in our previous study, 25 g of cleaned tin cans were cut into small pieces and dissolved in HNO_3 solution before NH_4OH solution was dropwise added till the formation of a reddish-brown precipitate. The precipitate was filtered, washed, dried, and finally calcined at 400 °C in static air for 3 h (Gomaa et al. 2023).

Preparation of Fe_2O_3-NiO composites

Four Fe_2O_3-NiO composites were prepared with different Fe_2O_3/NiO weight ratios (i.e., 0.7/0.3, 0.5/0.5, 0.2/0.8, and 0.1/0.9) by mixing Fe_2O_3 with nickel oxalate dihydrate. The theoretical calculations for the composite preparation are shown in Table 1. The calculated amounts of Fe_2O_3 and nickel oxalate dihydrate were well mixed with a small amount of deionized water and placed in an ultrasonic bath at 70 °C for 1 h. The resulting mixture was dried at 100 °C for 24 h and was finally calcined at 400 °C in static air for 2 h. The composites with Fe_2O_3/NiO ratios of 0.7/0.3, 0.5/0.5, 0.2/0.8, and 0.1/0.9 were labeled as 7Fe_2O_3-3NiO, 5Fe_2O_3-5NiO, 2Fe_2O_3-8NiO, and 1Fe_2O_3-9NiO, respectively.

Catalyst characterization

Thermogravimetric and differential thermal analyses (TGA/DTA) were performed on the parent materials in dry N_2 with a flowing rate of 40 mL/min and a heating rate of 10 °C/min using an automatic recorder model 50H Shimadzu thermal analyzer, made in Japan. Using Nicolet Omnic software, a Magna-FT-IR 500 (USA) in the wave number range of 4000–300 cm^{-1}, and the KBr disk technique, FT-IR spectra of the calcined samples were recorded. A model D5000 Siemens diffractometer (Germany) was used to perform X-ray powder diffraction (XRD) analysis. It was fitted with a copper anode that provided Ni-filtered Cu Kα radiation ($\lambda = 1.5406$ Å), with a 2θ range of 20 to 80°. For phase identification purposes, an automatic JCPDS library search and match (Diffrac software, Siemens) was made possible through an online data collecting and handling system. The crystallite size of the samples was calculated using Debye-Scherer's Eq. 1 (Tasisa et al. 2024)

$$D = K\lambda/(\beta\cos\theta) \tag{1}$$

in which D is the crystallite size (nm), λ is the wavelength (0.15412 nm), K is the shape factor (0.90), θ is the Bragg angle (radian), and β is the adjusted full width at half maximum (radian). The actual amounts of Fe and Ni in the composites were analyzed by inductively coupled plasma atomic emission spectrometry (ICPS, Shimadzu), after dissolving 5 mg of the sample in diluted aqua regia. The BET surface area measurements were carried out with an automatic Gemini (VIχ) Micromeritics (USA) Model 2390P at liquid nitrogen temperature (-195 °C). Prior to the measurements, the catalysts were outgassed for 1 h at 200 °C. Scanning electron microscopy (SEM) was used to analyze

Table 1 Theoretical calculations for the preparation of Fe_2O_3-NiO composites, ICP analysis results, and results of thermal analysis of the parent materials

Catalyst	Preparation calculations				ICP analysis of the composites		Thermal analysis results				
	Weight (g) of precursors		Wt. (%) of oxides after calcinations (a*)		%Ni	%Fe	Step (1) dehydration		Step (2) decomposition		%Total mass loss
	$NiC_2O_4.2H_2O$	Fe_2O_3	%NiO	%Fe_2O_3			Mass loss%	T_{max}/ °C	T_{max}/ °C	%Mass loss	
NiO	10	-	100	-	78.12	-	21.4	263	378	39.5	60.9
1Fe_2O_3-9NiO	9.5	0.5	88.1	11.9	69.10	8.10	20.9	255	383	37.1	58
2Fe_2O_3-8NiO	9	1	77.9	22.1	60.91	15.19	19.4	258	385	34.6	54
5Fe_2O_3-5NiO	7	3	47.7	52.3	36.92	36.34	16.1	254	386	26.4	42.5
7Fe_2O_3-3NiO	5	5	28.1	71.9	21.88	49.14	12.37	251	388	18.53	30.9
Fe_2O_3	-	10	-	100	-	68.71	-	-	-	-	-

a*These theoretical calculations were based on the TGA analysis results in which the total mass loss of $NiC_2O_4.2H_2O$ after calcination was 60.9% of its original weight

the surface morphology of the calcined samples using the JEOL JSM-IT200 SEM at different magnifications depending on the appearance of each sample. The EDAX quantitative elemental analysis was carried out for tin can waste and the recovered Fe_2O_3 using a Jeol JSX-3222 element analyzer system equipped with an X-ray tube of Rh anode.

Determination of surface basicity of the catalysts

The surface basic site densities were studied quantitatively and qualitatively using desorption thermogravimetry of CO_2 as an acidic probe molecule (TPD-TGA). Fifty milligrams of each sample was pre-activated by heating at 400 °C in static air for 1 h and then kept for 2 weeks in a glass chamber fitted with a gas inlet and outlet under a flow of 40 mL/min CO_2. Twenty to thirty milligrams of the sample saturated with CO_2 was subjected to TGA analysis in a nitrogen atmosphere under a heating rate of 20 °C/min from 30 to 400 °C. The percentage weight loss from TGA due to CO_2 desorption from the basic sites was calculated and used to determine the surface basic site densities. The density of basic sites as site/g was calculated using the following equation (Gomaa et al. 2021, 2023):

$$\text{Basic site density (site/g)} = \frac{\text{Moles of CO}_2 \text{ desorbed} \times \text{Avogadro Number (site / mol)}}{\text{Weight of sample } (g)}$$

(2)

Catalytic activity measurements

2-butanol dehydrogenation reaction was utilized to test the catalytic efficiency of the produced catalysts in a continuous-flow fixed-bed reactor operated at atmospheric pressure. The reaction was performed in a Pyrex glass reactor using 0.2 g of the catalyst. Prior to the reaction, the catalyst was preheated at 400 °C for 1 h under a flow of 100 mL/min N_2 to activate the catalyst's surface. After the activation step, the reactor temperature was adjusted to the desired reaction temperature, and the flow was switched to 100 mL/min of the reaction feed, which consisted of 0.789% of 2-butanol and 99.211% of N_2. The reactor output was recorded and analyzed using a gas chromatograph conducted with a data processing system model Shimadzu Chromatopac C-R4AD (Japan). The % conversions of 2-butanol and the selectivity to MEK were calculated using the following equations:

$$\%\text{Conversion} = \left[\frac{(\text{PA(standard)} - \text{PA(unreacted)})}{\text{PA(standard)}} \right] \times 100$$

(3)

$$\%\text{Selectivity(MEK)} = \left[\frac{\text{PA(MEK)}}{(\text{PA(MEK)} + \text{PA(Trans} - \text{butene)} + \text{PA(Cis} - \text{butene)})} \right] \times 100$$

(4)

where $\text{PA}_{\text{standard}}$ = standard peak area of 2-butanol; $\text{PA}_{\text{unreacted}}$ = peak area of the unreacted 2-butanol.

Results and discussion

Characterization of the catalysts

The parent materials, including nickel oxalate dihydrate, and the mixtures of nickel oxalate dihydrate with Fe_2O_3 were exposed to TGA and DTA analyses to analyze their thermal characteristics and detect the suitable calcination temperatures to form stable composites. Figures 1a and b show the TGA and DTA curves. All the TGA curves show two weight losses, which can be attributed to the thermal decomposition of Ni-Oxal, where the pre-calcined Fe_2O_3 is thermally stable within this temperature range (Mohamed et al. 2005; Chenakin and Kruse 2019; Gomaa et al. 2021). The first mass loss is attributed to the dehydration of $NiC_2O_4.2H_2O$ to NiC_2O_4, while the second is due to the decomposition of NiC_2O_4 to form NiO (Mohamed et al. 2005; Chenakin and Kruse 2019). As expected, the mass loss in the two TGA steps decreased by increasing the weight ratio of Fe_2O_3 at the expense of Ni-Oxal. Similar to TGA, DTA curves exhibit two endothermic peaks, which correspond to the same dehydration and decomposition steps (Donia 1997). By increasing the ratio of Fe_2O_3 in the mixtures, the first endothermic peak was slightly shifted towards lower temperature, while the second endothermic peak was slightly shifted towards higher temperatures. This indicates that increasing the dilution of Ni-Oxal with Fe_2O_3 seems to accelerate the dehydration step and delay the decomposition step of nickel oxalate, as mentioned in Table 1.

Figure 2A shows the FT-IR spectra of Fe_2O_3-NiO composites in comparison with pure NiO and Fe_2O_3 oxides. The broad band at 3400 cm^{-1} was related to ν(OH), and the band centered at 436 cm^{-1} was related to Ni–O bond vibrations (Mala et al. 2023). The two peaks centered at 1378 cm^{-1} and 1634 cm^{-1} were related to the uni- and bidentate surface carbonate adsorbed as CO_2 from the atmosphere (Donia 1997; Li et al. 2001). The small band at 420 cm^{-1}, which started to appear in the spectrum (d) and became more distinguishable by increasing the Fe_2O_3 ratio in the composites, can be attributed to Fe–O bond vibrations (Abdelrahman et al. 2019; Onizuka and Iwasaki 2022). A clear decrease was observed in the bands' intensity that was attributed to surface hydroxyl groups and adsorbed CO_2 by increasing the ratio of Fe_2O_3, indicating a decrease in the number of surface basic site densities.

The XRD diffractograms of Fe_2O_3, NiO, and Fe_2O_3-NiO composites are shown in Fig. 2B. The XRD pattern of NiO is composed of five diffractions indexed as (111), (200), (220), (311), and (222) crystal planes, corresponding to the cubic phase of NiO (JCPDS card no. 78–0423) (Wang et al. 2017; Rashad et al. 2020; Mala et al. 2023). The XRD pattern of Fe_2O_3 corresponds to hematite α-Fe_2O_3 (Rhombohedral) indexed to (JCPDS card no. 33–0664) with diffractions indexed as (012), (104), (110), (113), (024), (116), (018),

Fig. 1 TGA (**A**) and DTA (**B**) curves of pure nickel oxalate dihydrate (a) and nickel oxalate dihydrate mixed with x wt.% of Fe$_2$O$_3$ (x = 5, 10, 30, 50), (b, c, d, e) respectively, carried out in 40 mL/min of dry N$_2$ at a heating rate of 10 °C/min
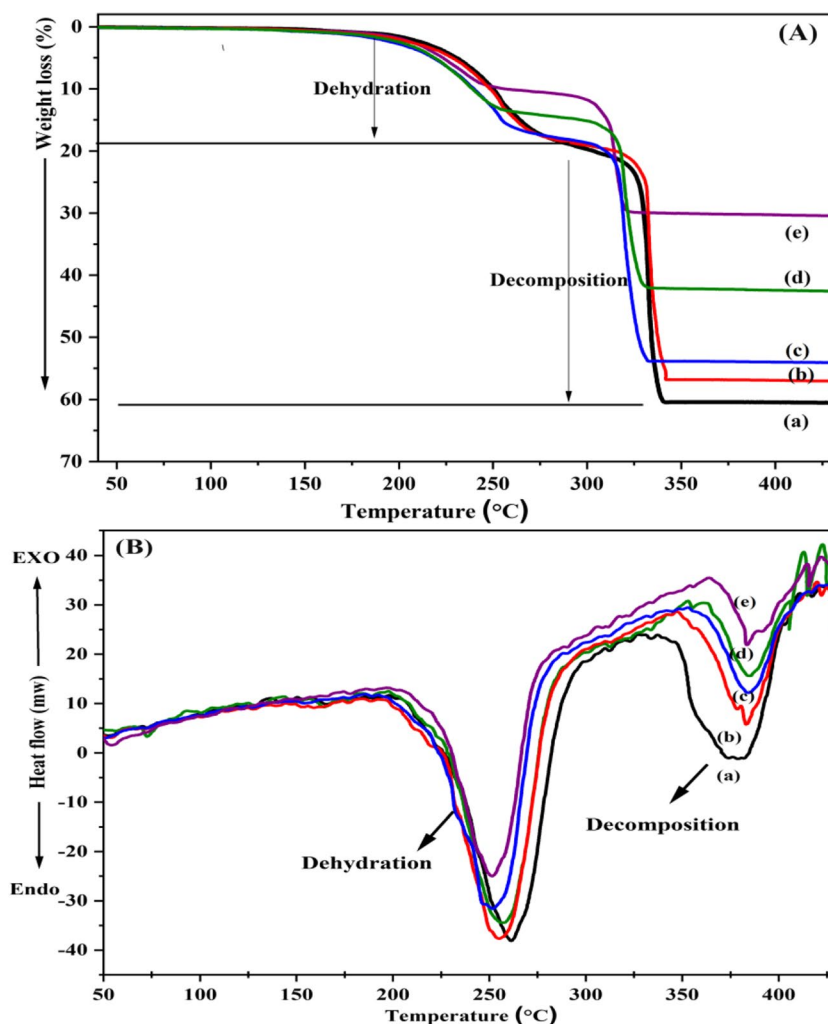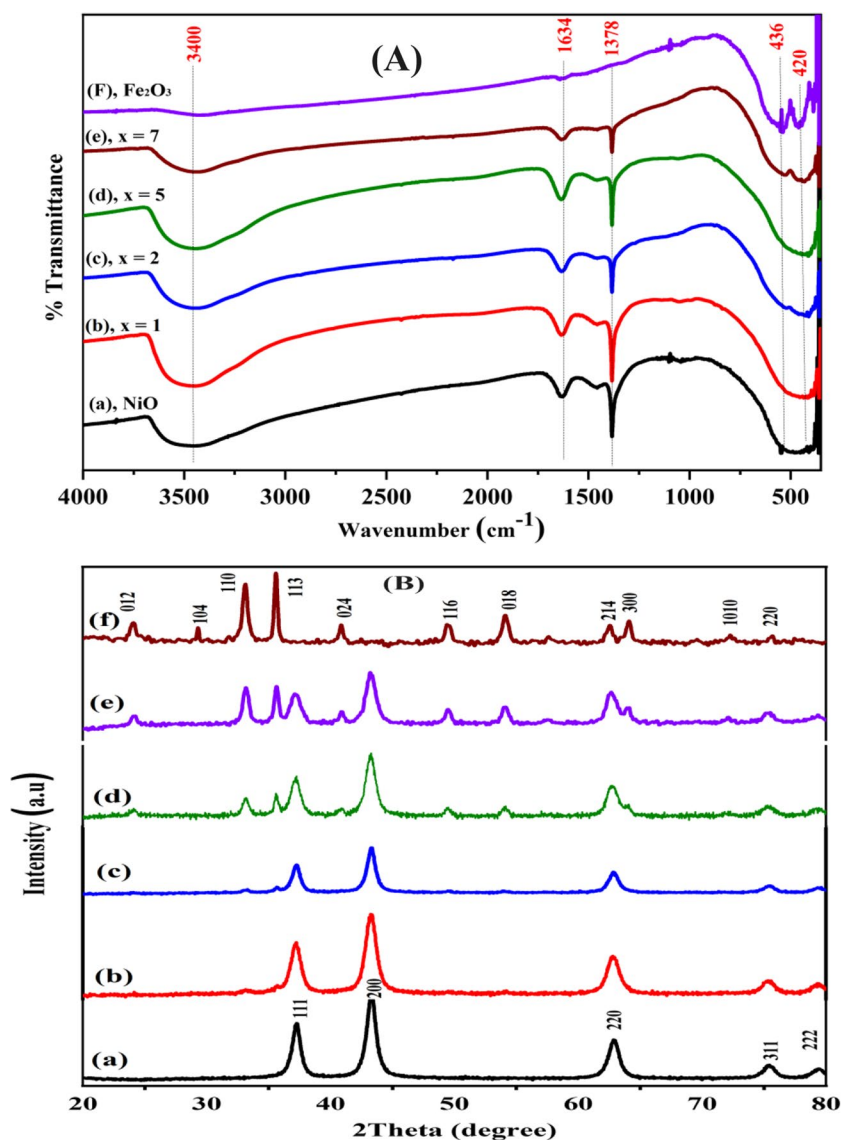

(214), and (330) (Abdelrahman et al. 2019; Ge et al. 2022). All the diffraction peaks of Fe$_2$O$_3$-NiO composites could be well indexed to cubic NiO (JCPDS card no. 78–0423) and rhombohedral α-Fe$_2$O$_3$ (JCPDS card no. 33–0664) with different intensities depending on the Fe$_2$O$_3$/NiO ratios (Wang et al. 2014; Bai et al. 2020; Dong et al. 2020). No characteristic diffraction peaks related to phases like Ni-metal, Fe-metal, or nickel–iron alloy could be observed, indicating that the final composites contain mainly mixtures of Fe$_2$O$_3$ and NiO. The ICP analysis was used to determine the actual percentages of Fe and Ni, revealing that the % of Fe and Ni at all composite ratios were in good agreement with the theoretical calculations as shown in Table 1.

The morphological structure of the calcined samples was identified using SEM analysis, as indicated in Fig. 3. It was found that NiO appears as a one-dimensional rod-like morphology with a relatively rough surface (Anandan and Rajendran 2011; Li et al. 2023), while Fe$_2$O$_3$ showed aggregates of irregular shapes. The SEM images of Fe$_2$O$_3$-NiO composites indicated that all composite images

had two types of particles, each one has its own appearance and are existing together in a random distribution. The first type of particles was that of rod morphology, which was attributed to NiO, while the second one was that of agglomerated particles of irregular shape, which was related to Fe$_2$O$_3$. As shown from SEM images of the mixed oxides, the two types of particles exist together in different ratios depending on the Fe$_2$O$_3$/NiO ratio without the formation of any new phases or spinals like NiFe$_2$O$_4$. As concluded by XRD analysis, the low calcination temperature of these samples was not enough for the formation of any spinals. Table 2 shows the crystallite sizes of the prepared catalysts calculated using the Scherrer equation from the XRD diffractograms. In addition, Table 2 also shows the surface area measurements, containing the total surface area, external surface area, and micropore area of Fe$_2$O$_3$, NiO, and Fe$_2$O$_3$-NiO composites. Comparing with Fe$_2$O$_3$, the surface area has been improved by the addition of NiO, especially at high ratios of NiO. This was attributed to the effect of sonication used during the preparation

steps of the mixed oxides, in addition to the effect of gas evolution during the dehydration and decomposition of Ni-Oxal in these mixtures (Halawy et al. 2022). In comparison with NiO, except for 1Fe$_2$O$_3$-9NiO, the surface area of the produced mixtures was slightly reduced by the replacement of NiO with Fe$_2$O$_3$.

Assessment of basic site densities

The basic site densities of the calcined samples were measured using the TGA-TPD technique of CO$_2$ to calculate the basic site density for each catalyst and to detect the different types of basic sites depending on their strengths as weak, medium, and strong. The acidic CO$_2$ molecule has been proposed as a suitable probe molecule due to its highly acidic nature, which can form stable adducts with a large variety of surface O^{2-} sites with different potential interactions. The desorbed amount of CO$_2$ at the given temperature range provides the concentration of basic sites, whereas the temperature is indicative of the basic strength of the site. Three types of basic sites were detected, including weak (< 125 °C), medium (125–275 °C), and strong (275–400 °C) (Gomaa et al. 2021, 2023). Figure 4a and Table 2 show the total number of basic sites over the pure oxides and the composite catalysts. NiO exhibited a higher density of basic sites (4.283×10^{20} site/g) compared to Fe$_2$O$_3$ (2.886×10^{20} site/g). Then, the surface basicity was improved by mixing Fe$_2$O$_3$ with NiO, as for all the composite catalysts except 7Fe$_2$O$_3$-3NiO, the total surface basicity was higher than that of the pure oxides. Based on the total number of surface basic sites, the prepared samples are arranged in the following order: 1Fe$_2$O$_3$-9NiO > 2Fe$_2$O$_3$-8NiO > 5Fe$_2$O$_3$-5NiO > NiO > 7Fe$_2$O$_3$-3NiO > Fe$_2$O$_3$. This arrangement of the samples according to their values

Fig. 3 SEM images of NiO (**a**), [xFe2O3-(10- x) NiO], where *x* (1, 2, 5, 7), (**b**, **c**, **d**, **e**), and Fe2O3 (**f**), respectively
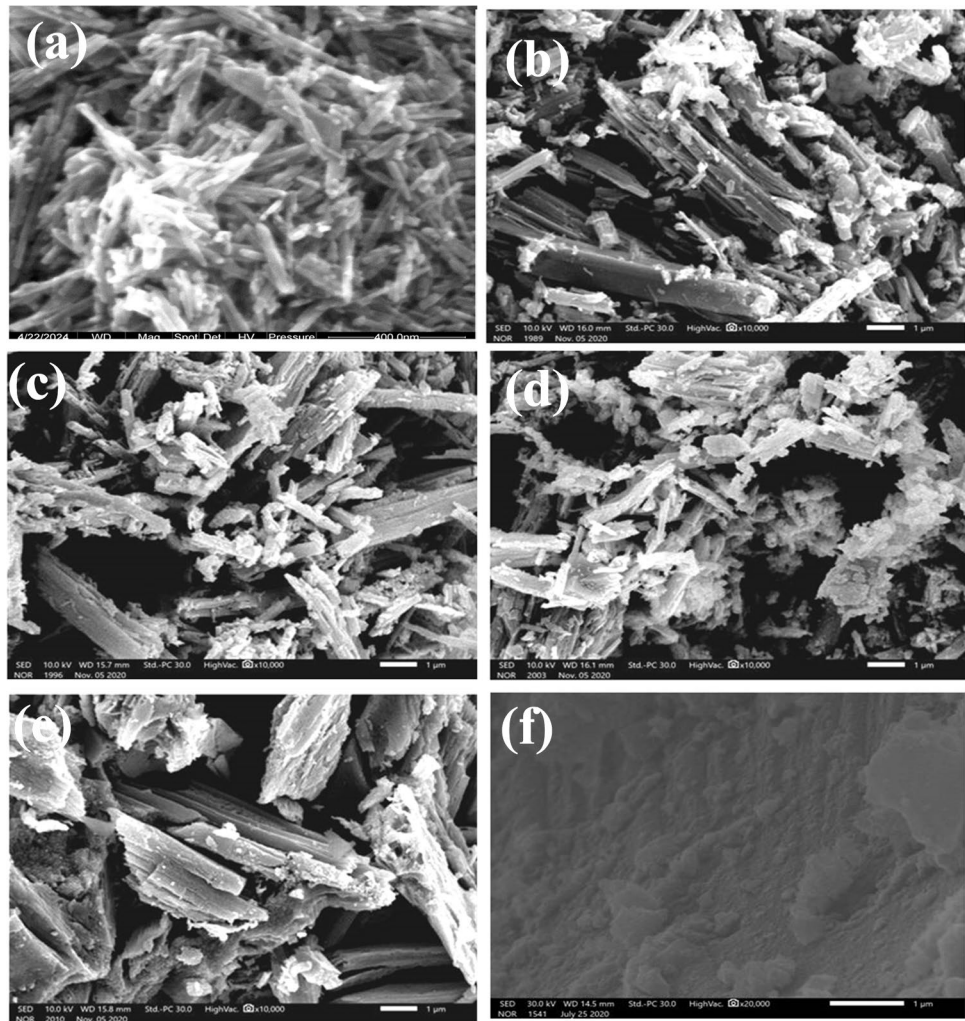

Table 2 Crystallite size, total S_{BET} (m^2/g), external S_{BET} (m^2/g), micropore area (m^2/g), and the total number of basic sites (site/g) and their distributions for all catalysts under investigations

Sample	Crystallite size (nm)	Total S_{BET} (m^2/g)	External S_{BET} (m^2/g)	Micropore area (m^2/g)	Total basic sites (site/g)	%WBS[1]	MBS[2]%	%SBS[3]
NiO	11.65	68.98	66.35	2.63	4.283×10^{20}	27.10	62	10.90
1Fe$_2$O$_3$-9NiO	9.82	88.67	87.53	1.455	6.036×10^{20}	31.95	51.1	16.70
2Fe$_2$O$_3$-8NiO	12.60	59.90	58.56	1.185	4.809×10^{20}	31.73	53.2	14.84
5Fe$_2$O$_3$-5NiO	10.22	66.31	65.16	1.149	4.840×10^{20}	29.66	52.4	17.37
7Fe$_2$O$_3$-3NiO	10.69	58.32	57.29	1.027	3.657×10^{20}	27.11	54	19.66
Fe$_2$O$_3$	22.45	48.73	46.12	2.609	2.886×10^{20}	21.20	40.9	37.90

[1]Weak basic sites

[2]Medium basic sites

[3]Strong basic sites

of surface basic sites indicated a strong mutual effect of both pure oxides, which had been proven previously by the intensity of adsorbed CO_2 peaks in FT-IR spectra. The formation of composites from these oxides strongly improved their basic surface densities compared to the pure oxides. Additionally, the primary type of basic site present on the surface of all samples was the medium type (bidentate carbonate), which desorbs in the temperature range of
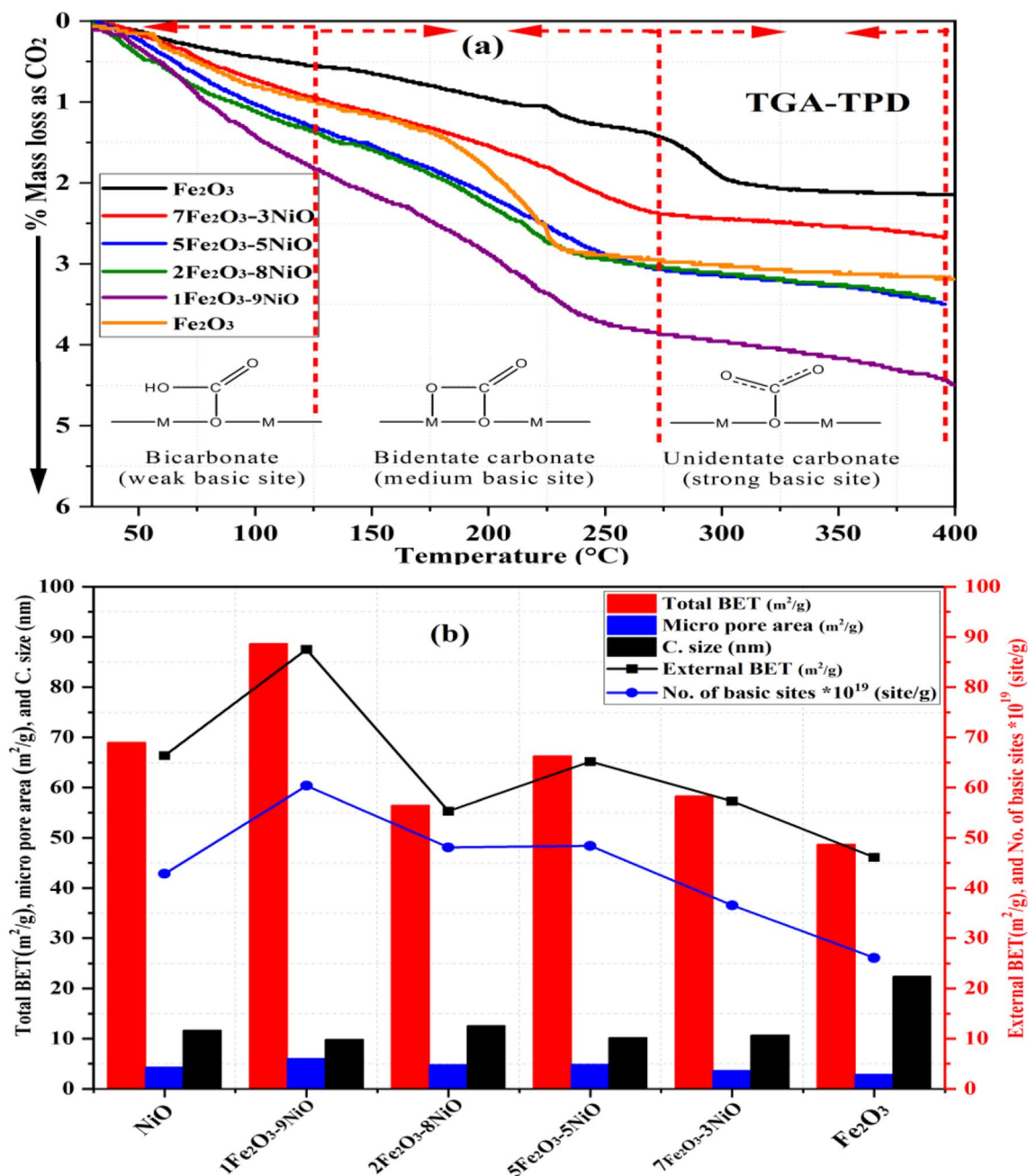
Fig. 4 CO_2 desorption thermogravimetry curves recorded for pure oxides and composites performed in 40 mL/min dry N_2 with 20 °C/min heating rate (**a**) and the relation between the surface properties of pure and composite samples (**b**)

125–275 °C. These sites are considered the most crucial type of basic sites for the dehydrogenation of 2-butanol to MEK (Gomaa et al. 2021; Halawy et al. 2022). Figure 4b illustrates the relationship among the surface texture properties of all prepared catalysts. For all the catalysts, the surface basicity of the catalysts exhibits a similar trend to that of total surface area and crystallite size. This similarity is likely due to the same reasons that depend mainly on the Fe_2O_3/NiO ratio in the composites.

Catalytic activity measurements

Effect of reaction temperature and catalyst composition

Figure 5a shows the relation between catalyst composition and conversion of 2-butanol at different reaction temperatures in the range of 250–325 °C. For all catalysts, the % conversion of 2-butanol increased by increasing the reaction temperature. This can be attributed to increasing the

kinetic energy of the reacting molecules, which enhanced their interaction, leading to a higher conversion rate (Halawy et al. 2018, 2021, 2022; Gomaa et al. 2021). Figure 5b shows the relation between catalyst composition and the selectivity of MEK at different reaction temperatures. The selectivity to MEK was slightly decreased by increasing the reaction temperature over all catalysts. However, the selectivity to MEK was higher than 85% for all catalysts at all reaction temperatures. Depending on the results presented in Fig. 5a, the catalysts can be arranged according to their catalytic activity as follows: $1Fe_2O_3$-$9NiO > NiO > 5Fe_2O_3$-$5NiO \geq 2Fe_2O_3$-$8NiO > 7Fe_2O_3$-$3NiO > Fe_2O_3$. This arrangement is in line with the arrangement of these catalysts according to total surface area, total number of basic sites, and crystallite size, as shown in Table 2. However, more explanation of the effects of Fe_2O_3 and NiO on each other is required.

Regarding the two pure oxides, it is clear from Fig. 5a that the catalytic activity of NiO is much higher than that of Fe_2O_3. The catalytic activity difference between the two oxides can be attributed to many reasons, such as the surface area, the surface basicity, and the chemical nature of each oxide. Regarding the mixed oxide catalysts and starting from the side of pure Fe_2O_3, the addition of NiO to Fe_2O_3 strongly improved the catalytic activity in a steady way by increasing the amount of NiO. This observation can be understood simply as a result of the gradual replacement of the Fe_2O_3 with low catalytic activity by the NiO with high catalytic activity. Whereas starting from the side of pure NiO, the addition of a small amount of Fe_2O_3 to NiO increased the catalytic activity, as in $1Fe_2O_3$-$9NiO$, and then the excess addition of Fe_2O_3 decreased the catalytic activity. Furthermore, the addition of Fe_2O_3 reduced the coke formation over the catalyst surface from a 30% weight gain of carbonaceous species in the case of pure NiO to almost zero in all Fe_2O_3-NiO catalysts, as shown in Fig. 5c. This effect of Fe_2O_3 addition to NiO can be understood from the results of some previous studies. Kathiraser and his co-workers (2016) studied the steam reforming of biomass tar resulting from cellulose gasification using supported Ni–Fe bimetallic catalysts. They found that the addition of Fe to Ni-containing catalyst suppressed the carbon deposition rate by up to 2.5 times due to the oxygen-scavenging effect of Fe, which promotes carbon gasification while providing sufficient active Ni metal sites. However, they found that increasing Fe loading above 1 wt.% led to a decrease in the catalytic activity due to the decrease in the Ni active site numbers. Wang et al. (2011) studied the catalytic activity of Ni–Fe catalysts toward the steam reforming of tar from biomass pyrolysis. They found that Ni–Fe catalysts with the optimal composition were much active in comparison with the monometallic Ni and Fe catalysts. According to Wang and his co-workers, the addition of Fe

improved the number of Ni active centers and increased the coverage of oxygen atoms during steam reforming reactions. The oxygen atoms of Fe species can be supplied to Ni species to catalyze the reaction between oxygen species and coke species formed on Ni sites, which reduces coke formation. Wang and his coworkers reported that the addition of excess Fe species dropped the catalytic performance due to decreasing the concentration of Ni active centers at the catalyst surface, which cannot be compensated by the excess Fe addition. It was reported that one of the most crucial factors responsible for the catalytic performance of NiO for the dehydrogenation of 2-butanol was the presence of the Ni/NiO interface. It was found that Ni-metal facilitates the formation of H_2 from H-adsorbed over Ni/NiO nanoscale hetero-surfaces (Halawy et al. 2021; Gomaa et al. 2021). In light of the results of these previous studies, we might be able to give our explanation of the effect of the addition of Fe_2O_3 to NiO. The replacement of a small amount of NiO with Fe_2O_3 in $1Fe_2O_3$-$9NiO$ catalyst increased the number of active Ni metal sites, which increased the area of the Ni/NiO interface, and consequently, the catalytic activity towards MEK formation increased. By increasing the ratio of Fe_2O_3 at the expense of NiO, the catalytic performance decreased due to a decrease in the number of active Ni sites. Furthermore, the addition of Fe_2O_3 to NiO inhibited the coke formation over all the mixed oxide catalysts due to the oxygen-scavenging effect of Fe, which promotes the oxidation of the carbonaceous species (Wu et al. 2021; Kathiraser et al. 2016).

Effect of weight-hourly-space-velocity (WHSV)

The effect of WHSV on the catalytic efficiency of $7Fe_2O_3$-$3NiO$ was tested in reaction temperature range of 225–325 °C. Figure 6 shows the % conversion of 2-butanol and the selectivity to MEK over $7Fe_2O_3$-$3NiO$ at three different values of WHSV: 15, 30, and 60 $L.h^{-1}.g^{-1}$. Increasing the value of WHSV resulted in a remarkable decrease in the % conversion. This can be attributed to the decrease in contact or residence time between the reacting molecules and the active basic sites on the catalyst surface (Natesakhawat et al. 2015; Halawy et al. 2021; Gomaa et al. 2024). There is no effect of increasing the value of WHSV on the product selectivity, as shown in Fig. 6, which indicates that the selectivity to MEK is independent of the value of WHSV.

Catalytic stability and durability

To examine the catalytic stability and reusability of the $7Fe_2O_3$-$3NiO$ catalyst, four complete cycles of the reaction were carried out at a temperature range of 225–325 °C at WHSV of

Fig. 5 Relation between catalyst composition during 2-butanol dehydrogenation and **a** % conversion of 2-butanol, **b** MEK % selectivity, and **c** % coke formation at the spent catalyst
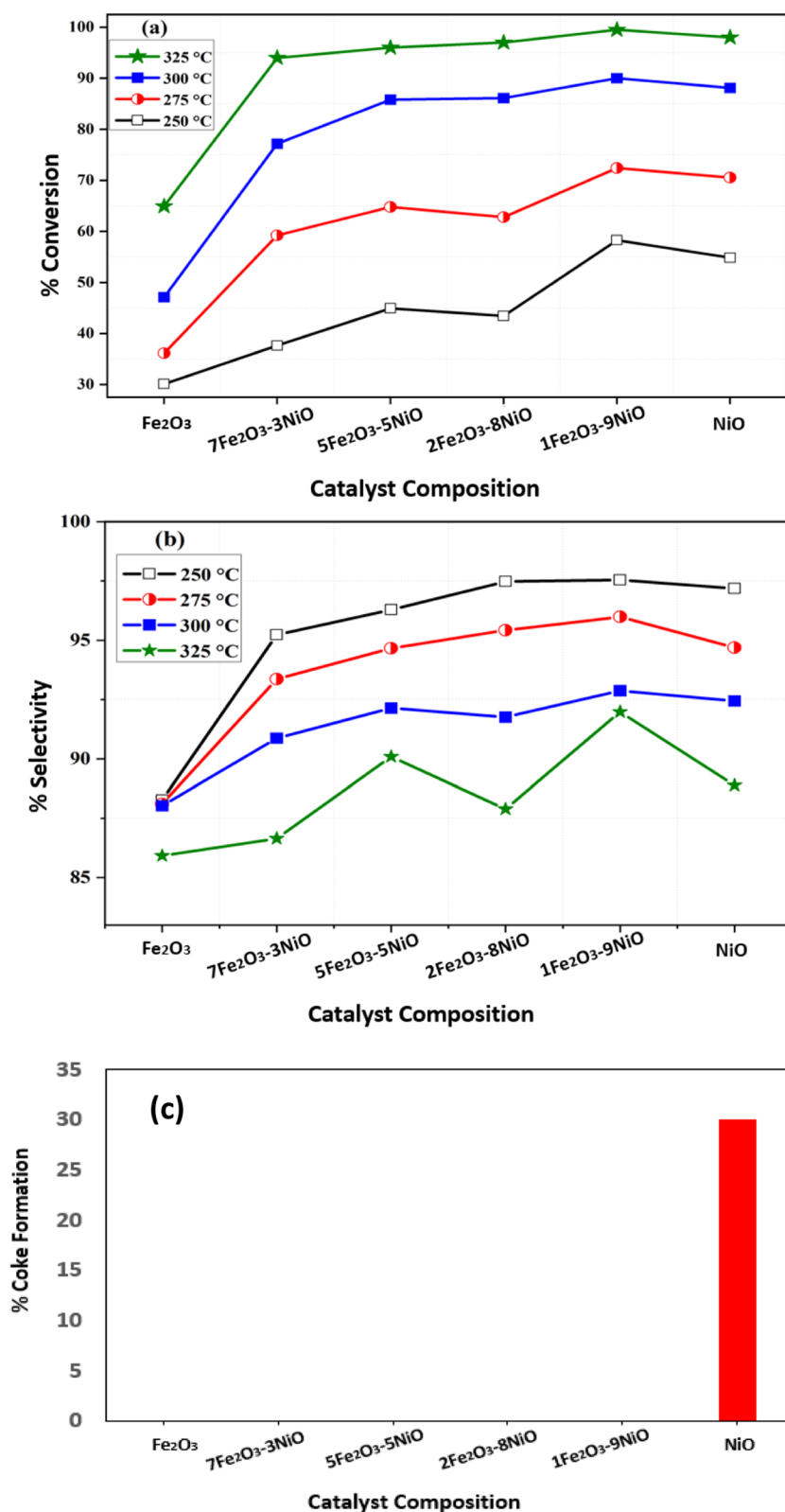
30 L.h^{-1}.g^{-1}. An activation step was performed prior to each cycle by heating the catalyst at 400 °C for 1 h under N$_2$ flow. In order to prevent any discrepancies during the reaction, specific conditions had been imposed, including catalyst weight, the exact reactor position inside the furnace, and the distribution of the catalyst inside the reactor (Gomaa et al. 2024). After four
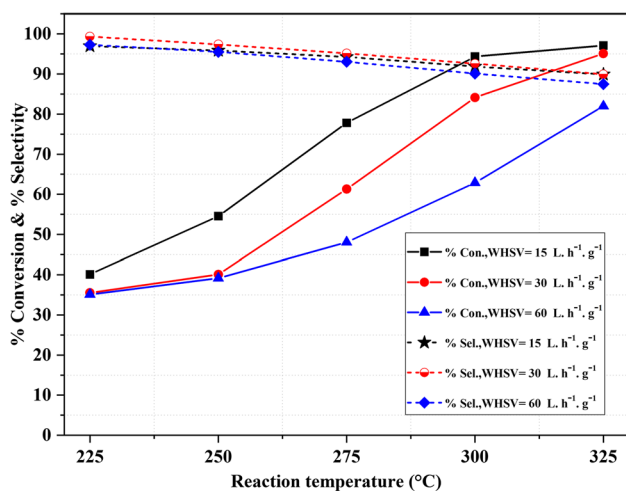
Fig. 6 % conversion of 2-butanol and % selectivity to MEK as a function of reaction temperature at different values of WHSV over $7Fe_2O_3$-3NiO catalyst
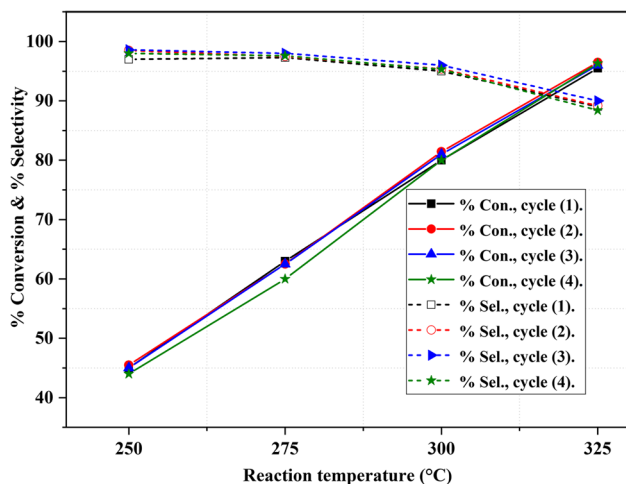
Fig. 7 Catalytic activity and selectivity profile of fresh and spent $7Fe_2O_3$–3NiO catalyst during 2-butanol dehydrogenation

cycles, the catalyst showed clear stability, both in the % conversion of 2-butanol and the selectivity to MEK as shown in Fig. 7. This indicates the sustained catalytic activity and selectivity of the catalysts due to the synergistic effect of the two oxides. This combination between NiO and Fe_2O_3 provides sufficient active sites for the reaction and prevents coke formation, which enhances the catalyst's resistance to deactivation.

Conclusion

Four Fe_2O_3-NiO composites with different Fe_2O_3/NiO ratios were prepared with an ultrasonic-assisted, environmentally friendly preparation method using only water as a solvent. The catalytic activity of these composites was tested in the dehydrogenation of 2-butanol to MEK and compared with that of pure iron and nickel oxides. The results indicated the superiority of the composites over the pure oxides due to the synergistic effect of the two oxides. While NiO provides most of the active surface basic sites, Fe_2O_3 prevents coke formation by the oxygen-scavenging effect of Fe, which promotes the oxidation of the carbonaceous species. This synergistic effect between the two oxides produces catalysts with better catalytic activity and better stability compared to the pure iron and nickel oxides. The optimum mixing ratio of the two oxides was $1Fe_2O_3$:9NiO, which shows the highest surface area, the highest total number of surface basic site, and the lowest value of crystallite size. Furthermore, this catalyst was the most active and selective to MEK compared to the other catalysts. We strongly recommend the NiO-Fe_2O_3 system for the production of MEK through 2-butanol dehydrogenation.

Declarations

Ethics approval This article does not contain any studies with human or animal subjects.

Consent to participate All authors agreed to participate in this study.

Consent for publication All authors agreed to publish this article.

Competing interests The authors declare no competing interests.

References

Abdelrahman EA, Hegazey RM, Kotp YH, Alharbi A (2019) Facile synthesis of Fe_2O_3 nanoparticles from Egyptian insecticide cans for efficient photocatalytic degradation of methylene blue and crystal violet dyes. Spectrochim Acta A Mol 222:117195. https://doi.org/10.1016/j.saa.2019.117195

Anandan B, Rajendran V (2011) Morphological and size effects of NiO nanoparticles via solvothermal process and their optical properties. Mater Sci Semicond 14:43–47. https://doi.org/10.1016/j.mssp.2011.01.001

Bai S, Han J, Han N, Zhang K, Sun J, Sun L, Luo R, Li D, Chen A (2020) An α-Fe_2O_3/NiO p-n hierarchical heterojunction for the sensitive detection of triethylamine. Inorg Chem Front 7:1532–1539. https://doi.org/10.1039/C9QI01548E

Bharathiraja B, Jayamuthunagai J, Sudharsanaa T, Bharghavi A, Praveenkumar R, Chakravarthy M, Yuvaraj D (2017) Biobutanol-an impending biofuel for future: a review on upstream

and downstream processing techniques. Renew Sust Energ Rev 68:788–807. https://doi.org/10.1016/j.rser.2016.10.017

Bolder FHA (2008) Dehydrogenation of alcohol mixtures to esters and ketones. Ind Eng Chem Res 47:7496–7500. https://doi.org/10.1021/ie800667p

Chenakin S, Kruse N (2019) Thermal decomposition of nickel oxalate dihydrate: a detailed XPS insight. J Phys Chem C 123:30926–30936. https://doi.org/10.1021/acs.jpcc.9b07879

Dong S, Wu D, Gao W, Hao H, Liu G, Yan S (2020) Multi-dimensional templated synthesis of hierarchical Fe_2O_3/NiO composites and their superior ethanol sensing properties promoted by nanoscale p-n heterojunctions. Dalton Trans 49:1300–1310. https://doi.org/10.1039/C9DT04185K

Donia AM (1997) Synthesis, identification and thermal analysis of co-precipitates of silver- (cobalt, nickel, copper and zinc) oxalate. Polyhedron 16:3013–3031. https://doi.org/10.1016/S0277-5387(97)00041-7

Fang D, Ren W, Liu Z, Xu X, Xu L, Lü H, Zhang H (2009) Synthesis and applications of mesoporous $Cu-Zn-Al_2O_3$ catalyst for dehydrogenation of 2-butanol. J Nat Gas Chem 18:179–182. https://doi.org/10.1016/S1003-9953(08)60099-7

Gaigneaux EM, Tsiakaras PE, Herla D, Ghenne L, Ruiz P, Delmon B (1997) Catalytic synergy via spillover at low temperature: the dehydration and dehydrogenation of sec-butanol in the presence of oxygen. Catal Today 33:151–160. https://doi.org/10.1016/S0920-5861(96)00104-6

Gao K, Wang B, Tao L, Cunning BV, Zhang Z, Wang S, Ruoff RS, Qu L (2019) Efficient metal-free electrocatalysts from N-doped carbon nanomaterials: mono-doping and Co-doping. Adv Mater 31:1805121. https://doi.org/10.1002/adma.201805121

Ge T, Shen L, Li J, Zhang Y, Zhang Y (2022) Morphology-controlled hydrothermal synthesis and photocatalytic Cr (VI) reduction properties of α-Fe_2O_3. Colloids Surf a: Physicochem Eng Asp 635:128069. https://doi.org/10.1016/j.colsurfa.2021.128069

Geravand E, Shariatinia Z, Yaripour F, Sahebdelfar S (2015) Synthesis of copper–silica nanosized catalysts for 2-butanol dehydrogenation and optimization of preparation parameters by response surface method. Chem Eng Res Des 96:63–77. https://doi.org/10.1016/j.cherd.2015.02.003

Gomaa AA, Halawy S, Abdelkader A (2021) Preparation and characterization of nanocrystalline NiO by the thermal decomposition of oxalate salts for the dehydrogenation of 2-butanol to methyl ethyl ketone. Asw Uni J Env S 2:178–189. https://doi.org/10.21608/aujes.2021.77260.1025

Gomaa AA, Osman AI, Halawy SA, Mohamed MA, Abdelkader A (2023) Synthesis of highly basic, low-cost iron oxides from tin can waste as valorization of municipal solid waste and study of their catalytic efficiency as potent catalysts for MEK production. J Mater Cycles Waste Manag 26:882–893. https://doi.org/10.1007/s10163-023-01865-8

Gomaa AA, Abdelkader A, Khodari M (2024) Highly acidic, γ-Al_2O_3 nanorods and SiO_2 nanoparticles recovered from solid wastes as promising catalysts for production of ethylene and diethyl ether biofuels. Waste Biomass Valor. https://doi.org/10.1007/s12649-024-02518-z

Guan Y, Liu Y, Song H, Wang B, Zhang G, Wang Y (2024) High-reactive and coke-resistant polyhedral NiO/Fe_2O_3 oxygen carrier for enhancing chemical looping CH_4–CO_2 dry reforming. J Clean Prod 447:141490. https://doi.org/10.1016/j.jclepro.2024.141490

Halawy SA, Mohamed MA, Abdelkader A (2018) Hierarchical nanocrystalline NiO with coral-like structure derived from nickel galactarate dihydrate: an active mesoporous catalyst for methyl ethyl ketone production. Arab J Chem 11:991–999. https://doi.org/10.1016/j.arabjc.2018.03.023

Halawy SA, Osman AI, Abdelkader A, Yang H (2021) Boosting NiO catalytic activity by x wt.% F-ions and K_2O for the production of methyl ethyl ketone (MEK) via catalytic dehydrogenation of 2-butanol. Chem Cat Chem 13:2200–2214. https://doi.org/10.1002/cctc.202001954

Halawy SA, Osman AI, Rooney DW (2022) Highly basic and active ZnO–x% K_2O nanocomposite catalysts for the production of methyl ethyl ketone biofuel. Energy Sci Eng 10:2827–2841. https://doi.org/10.1002/ese3.1171

Hoppe F, Burke U, Thewes M, Heufer A, Kremer F, Pischinger S (2016) Tailor-made fuels from biomass: potentials of 2-butanone and 2-methylfuran in direct injection spark ignition engines. Fuel 167:106–117. https://doi.org/10.1016/j.fuel.2015.11.039

Kathiraser Y, Ashok J, Kawi S (2016) Synthesis and evaluation of highly dispersed SBA-15 supported Ni–Fe bimetallic catalysts for steam reforming of biomass derived tar reaction. Catal Sci Technol 6:4327–4336. https://doi.org/10.1039/C5CY01910A

Kayo A, Yamaguchi T, Tanabe K (1983) The effect of preparation method on the acidic and catalytic properties of iron oxide. J Catal 83:99–106. https://doi.org/10.1016/0021-9517(83)90033-7

Kumar M, Gayen K (2011) Developments in biobutanol production: new insights. Appl Energy 88:1999–2012. https://doi.org/10.1016/j.apenergy.2010.12.055

Li GJ, Huang XX, Shi Y, Guo JK (2001) Preparation and characteristics of nanocrystalline NiO by organic solvent method. Mater Lett 51:325–330. https://doi.org/10.1016/S0167-577X(01)00312-3

Li F, Yan P, Herold F, Drochner A, Wang H, Cao T, Liu W, Dai X, Zhang B, Etzold BJM, Qi W (2020a) Oxygen assisted butanol conversion on bifunctional carbon nanotube catalysts: activity of oxygen functionalities. Carbon 170:580–588. https://doi.org/10.1016/j.carbon.2020.08.053

Li F, Dai X, Qi W (2020b) Primary amine coupling on nanocarbon catalysts: reaction mechanism and kinetics via fluorescence probe analysis. Green Energy Environ 5:5453–5460. https://doi.org/10.1016/j.gee.2020.09.008

Li L, Zhou L, Hu Z, Li T, Chen B, Li HY, Liu H (2023) Hollow-out Fe_2O_3-loaded NiO heterojunction nanorods enable real-time exhaled ethanol monitoring under high humidity. ACS App Mater Interface 15(12):15707–15720. https://doi.org/10.1021/acsami.2c23088

Mala NA, Dar MA, Rather MUD, Reshi BA, Sivakumar S, Batoo KM, Ahmad Z (2023) Supercapacitor and magnetic properties of NiO and manganese-doped NiO nanoparticles synthesized by chemical precipitation method. J Mater Sci: Mater Electron 34(6):505. https://doi.org/10.1007/s10854-023-09907-5

Mohamed MA, Galwey AK, Halawy SA (2005) A comparative study of the thermal reactivities of some transition metal oxalates in selected atmospheres. Thermochim Acta 429:57–72. https://doi.org/10.1016/j.tca.2004.08.021

Natesakhawat S, Means NC, Howard BH, Smith M, Abdelsayed V, Baltrus JP, Cheng Y, Lekse JW, Link D, zorreale BD, (2015) Improved benzene production from methane dehydroaromatization over Mo/HZSM-5 catalysts via hydrogen-permselective palladium membrane reactors. Catal Sci Technol 5:5023–5036. https://doi.org/10.1039/C5CY00934K

Onizuka T, Iwasaki T (2022) Low-temperature solvent-free synthesis of polycrystalline hematite nanoparticles via mechanochemical activation and their adsorption properties for Congo red. Solid State Sci 129:106917. https://doi.org/10.1016/j.solidstatesciences.2022.106917

Pischetola C, Collado L, Aguado-Molina R, Martín-Treceño S, Keane MA, Cardenas-Lizana F (2020) Continuous furfuryl alcohol production via coupled dehydrogenation-hydrogenation over supported Cu and Au catalysts: a consideration of hydrogen generation and transfer. Mol Catal 492:110912. https://doi.org/10.1016/j.mcat.2020.110912

Rashad M, Darwish AAA, Qashou SI, Abd El-Rahman KF (2020) Influence of ultraviolet irradiation on physical properties of

nano-NiO films for optical applications. Mater Res Bull 126:1–9. https://doi.org/10.1007/s00339-020-04012-4

Tasisa YE, Sarma TK, Sahu TK, Krishnaraj R (2024) Phytosynthesis and characterization of tin-oxide nanoparticles (SnO_2-NPs) from Croton macrostachyus leaf extract and its application under visible light photocatalytic activities. Sci Rep 14(1):10780. https://doi.org/10.1038/s41598-024-60633-2

Varma AR, Shrirame BS, Gadkari S, Vanapalli KR, Kumar V, Maity SK (2024) Techno-economic viability of bio-based methyl ethyl ketone production from sugarcane using integrated fermentative and chemo-catalytic approach: process integration using pinch technology. J Chem Eng 489:151297–151311. https://doi.org/10.1016/j.cej.2024.151297

Wang L, Li D, Koike M, Koso S, Nakagawa Y, Xu Y, Tomishige K (2011) Catalytic performance and characterization of Ni-Fe catalysts for the steam reforming of tar from biomass pyrolysis to synthesis gas. Appl Catal A 392:248–255. https://doi.org/10.1016/j.apcata.2010.11.013

Wang C, Cheng X, Zhou X, Sun P, Hu X, Shimanoe K, Lu G, Yamazoe N (2014) Hierarchical α-Fe_2O_3/NiO composites with a hollow structure for a gas sensor. ACS Appl Mater Interfaces 6:12031–12037. https://doi.org/10.1021/am501063z

Wang B, Shao H, Wang L, Yu R, Wang D (2017) Highly controlled synthesis of multi-shelled NiO hollow microspheres for enhanced lithium storage properties. Mater Res Bull 87:224–229. https://doi.org/10.1016/j.materresbull.2016.12.005

Wu L, Xie X, Ren H, Gao XA (2021) Short review on nickel-based catalysts in dry reforming of methane: influences of oxygen defects on anti-coking property. Mater Today Proc 42:153–160. https://doi.org/10.1016/j.matpr.2020.10.697

Zhang L, Chen C, Li X, Zhang Y (2024) Preparation and catalytic performance of the copper-manganese-silicon catalysts for dehydrogenation reaction of 2-butanol. JCS Pak 46(1):18–18

Zhenhua LIU, Wenzhou HUO, Hao MA, Kai QIAO (2006) Development and commercial application of methyl-ethyl-ketone production technology. Chin J Chem Eng 14:676–684. https://doi.org/10.1016/S1004-9541(06)60134-1